


## Elastic Geobarometry for Anisotropic Inclusions in Anisotropic Host Minerals: Quartz-in-Zircon

 Joseph P. Gonzalez<sup>1</sup> , Mattia L. Mazzucchelli<sup>1,2</sup> , Ross J. Angel<sup>3</sup>, and Matteo Alvaro<sup>1</sup>
<sup>1</sup>Department of Earth and Environmental Sciences, University of Pavia, Pavia, Italy, <sup>2</sup>Mainz Institute of Multiscale Modeling and Institute of Geosciences, Johannes-Gutenberg University of Mainz, Mainz, Germany, <sup>3</sup>IGG-CNR, Padova, Italy

### Key Points:

- A new model for elastic thermobarometry is presented that accounts for the elastic anisotropy and crystallographic orientation of minerals
- The anisotropic elastic model was used to evaluate the suitability of the quartz-in-zircon system for thermobarometric applications
- Isotropic elastic models cannot resolve the strain state of an elastically anisotropic inclusion in an elastically anisotropic host

### Supporting Information:

Supporting Information may be found in the online version of this article.

### Correspondence to:

M. L. Mazzucchelli,  
[mlmazzucchelli@gmail.com](mailto:mlmazzucchelli@gmail.com)

### Citation:

Gonzalez, J. P., Mazzucchelli, M. L., Angel, R. J., & Alvaro, M. (2021). Elastic geobarometry for anisotropic inclusions in anisotropic host minerals: Quartz-in-zircon. *Journal of Geophysical Research: Solid Earth*, 126, e2021JB022080. <https://doi.org/10.1029/2021JB022080>

Received 17 MAR 2021  
 Accepted 30 MAY 2021

**Abstract** Current models for elastic geobarometry have been developed with the assumption that the host and/or inclusion minerals are elastically isotropic. This assumption has limited applications of elastic thermobarometry to mineral inclusions contained in cubic quasi-isotropic host minerals (e.g., garnet). Here, we report a new elastic model that takes into account the anisotropic elastic properties and relative crystallographic orientation (RCO) of a host-inclusion system where both minerals are noncubic. This anisotropic elastic model can be used for host-inclusion elastic thermobarometric calculations provided that the RCO and elastic properties of both the host and inclusion are known. We then used this anisotropic elastic model to numerically evaluate the effects of elastic anisotropy and RCO on the strains and stresses developed in a quartz inclusion entrapped in a zircon host after exhumation from known entrapment  $P$ - $T$  conditions to room  $P$ - $T$  conditions. We conclude that the anisotropic quartz-in-zircon elastic model is suitable for elastic thermobarometry and may be widely applicable to crustal rocks. Our results demonstrate that isotropic elastic models cannot be used to determine the entire strain state of an elastically anisotropic inclusion contained in an elastically anisotropic host mineral, and therefore may lead to errors on estimated remnant inclusion pressures.

**Plain Language Summary** Minerals in rocks (re)crystallize at elevated pressures and temperatures within the Earth during geologic processes and often entrap other minerals within them as inclusions. These rocks may be eventually exhumed to the Earth's surface and can be directly observed. By determining the residual elastic deformation in the encapsulated inclusion, we can use an elastic model to estimate the pressure and temperature at which the inclusion was entrapped in its host, which gives information on the depth of host crystallization. However, minerals are generally elastically anisotropic, meaning that the elastic properties vary with direction within the crystal. Until now, elastic models have simplified calculations by assuming that the host and/or inclusion minerals are elastically isotropic. Here, we present a new model that accounts for this elastic anisotropy. Our results show that for common anisotropic host-inclusion mineral pairs, such as a quartz inclusion in a zircon host, the final strain in the inclusion depends on the elastic properties of the two minerals, and on their relative orientation. These results also imply that the previously used simplified isotropic models cannot determine the entire strain state of an anisotropic inclusion in an anisotropic host, and therefore may lead to errors on estimated inclusion pressures.

## 1. Introduction

Solid mineral inclusions entrapped within a host mineral can retain physical and chemical information from the pressure ( $P$ )-temperature ( $T$ ) conditions of entrapment and evolution during subsequent metamorphism. In addition to conventional thermobarometric methods (i.e., exchange thermobarometry, equilibrium assemblage modeling, etc.), application of elastic models to determine the metamorphic conditions of inclusion entrapment have become commonly used petrologic methods (e.g., Ashley et al., 2014; Enami et al., 2007; Gonzalez et al., 2019; Wolfe & Spear, 2020; Zhong et al., 2019), and can be used to constrain metamorphic processes when carefully applied. Elastic thermobarometric models are based on the premise that, in the absence of viscous reequilibration, isolated mineral inclusions retain elastic strains and stresses that can be used to calculate the  $P$ - $T$  conditions of entrapment within the host mineral (cf., Ferrero & Angel, 2018). If viscous relaxation of the strains or thermally induced shape change of the inclusion occurred during the metamorphic history, of course the determined strains will indicate the  $P$ - $T$  conditions of the

© 2021. The Authors.

This is an open access article under the terms of the [Creative Commons Attribution-NonCommercial License](https://creativecommons.org/licenses/by-nc/4.0/), which permits use, distribution and reproduction in any medium, provided the original work is properly cited and is not used for commercial purposes.

last elastic reequilibration event (e.g., Alvaro et al., 2020; Baldwin et al., 2021; Cesare et al., 2021; Moulas et al., 2020). Because of the near ubiquity of mineral inclusions, elastic thermobarometry has been applied to a variety of tectonic and petrologic problems such as garnet growth during subduction zone metamorphism (Ashley et al., 2014; Gonzalez et al., 2020), elastic reequilibration of inclusion strains (Alvaro et al., 2020; Baldwin et al., 2021; Zhong et al., 2018), and thermodynamic reaction overstepping (Spear & Wolfe, 2020; Spear et al., 2014).

Until now, elastic models (e.g., Angel et al., 2017b; Guiraud & Powell, 2006; Rosenfeld & Chase, 1961; Zhang, 1998) have been developed for cubic host minerals that contain cubic inclusion minerals with the explicit assumption that both are elastically isotropic. Such models have also been frequently used to calculate the entrapment conditions of elastically anisotropic inclusions contained within quasi-isotropic host minerals, for example, in the frequently applied quartz-in-garnet elastic model. However, it has been shown that when an inclusion is elastically anisotropic and contained within an isotropic host, the inclusion will develop nonhydrostatic stresses during exhumation (e.g., Angel et al., 2020; Mazzucchelli et al., 2019; Murri et al., 2018, Nestola, 2020; Zhong et al., 2019, 2020a). The full strain state of a natural inclusion can be determined using in-situ single crystal X-ray diffraction (SC-XRD) or Raman spectroscopy in conjunction with the phonon-mode Grüneisen tensors (Alvaro et al., 2020; Angel et al., 2019; Murri et al., 2018). Recently, a new model for elastic calculations has been reported that accounts for the elastic anisotropy of an anisotropic inclusion contained within a host with cubic crystallographic symmetry (Mazzucchelli et al., 2019). This elastic model uses the axial equation of state (EoS) of the inclusion and the volume EoS of the host to account for the elastic anisotropy of the inclusion and determine the remnant strain, stress and pressure developed in the inclusion upon exhumation (i.e.,  $P_{inc}$ ; Mazzucchelli et al., 2019). Alvaro et al. (2020) showed how this calculation can be inverted to estimate the unique  $P$ - $T$  conditions of inclusion entrapment.

Mineral inclusions are often contained within noncubic host minerals that will impose significant anisotropic elastic strains on the inclusion. The anisotropic strains imposed upon an elastically anisotropic inclusion by the elastically anisotropic host mineral depend in part on their relative crystallographic orientation (RCO). Recently, however, simple isotropic models have been applied to nonisotropic host minerals, such as quartz inclusions contained in epidote (Cisneros et al., 2020), apatite inclusions contained in zircon (Guo et al., 2021), and coesite inclusions contained in kyanite (Taguchi et al., 2019), implicitly assuming that the effect of the elastic anisotropy and RCO is negligible. The underlying assumption is that, even in these fully anisotropic systems, the values of the residual mean stress and the volume strain of the inclusion are the same as those obtained from a purely isotropic model. However, this assumption has never been evaluated or tested theoretically or experimentally, and if these simple models do not correctly describe the behavior of the elastically anisotropic host-inclusion system, their results may lead to incorrect geological interpretations.

Here, we introduce a new elastic model that takes into account the anisotropic elastic properties of a host-inclusion system where both minerals are noncubic. Since elastically anisotropic zircon is a common constituent of crustal rocks and frequently contains elastically anisotropic quartz inclusions, we evaluated the anisotropic elastic model in a series of computational tests in which a quartz inclusion is “entrapped” in a zircon host at several ranges of  $P$ - $T$  conditions corresponding to the eclogite, amphibolite, and granulite facies. The anisotropic elastic model is used to quantify and describe the orientation-dependent elastic interactions between the elastically anisotropic quartz inclusion and the elastically anisotropic zircon host to determine the remnant strains, stresses, and pressure preserved within the inclusion at room  $P$ - $T$  conditions. The quartz-in-zircon elastic model that we have developed is potentially widely applicable to crustal rocks and provides the theoretical basis for expanding elastic thermobarometry to other fully anisotropic host-inclusion systems.

## 2. Background

Elastic anisotropy of a mineral describes the variation of its elastic properties as a function of the direction within the crystal. In general, all minerals (including cubic minerals) are anisotropic with respect to their elastic properties (Nye, 1985). Because of this, noncubic minerals develop anisotropic strains even under hydrostatic pressure. Therefore, even if the load (e.g., lithostatic pressure) on the host mineral is assumed to

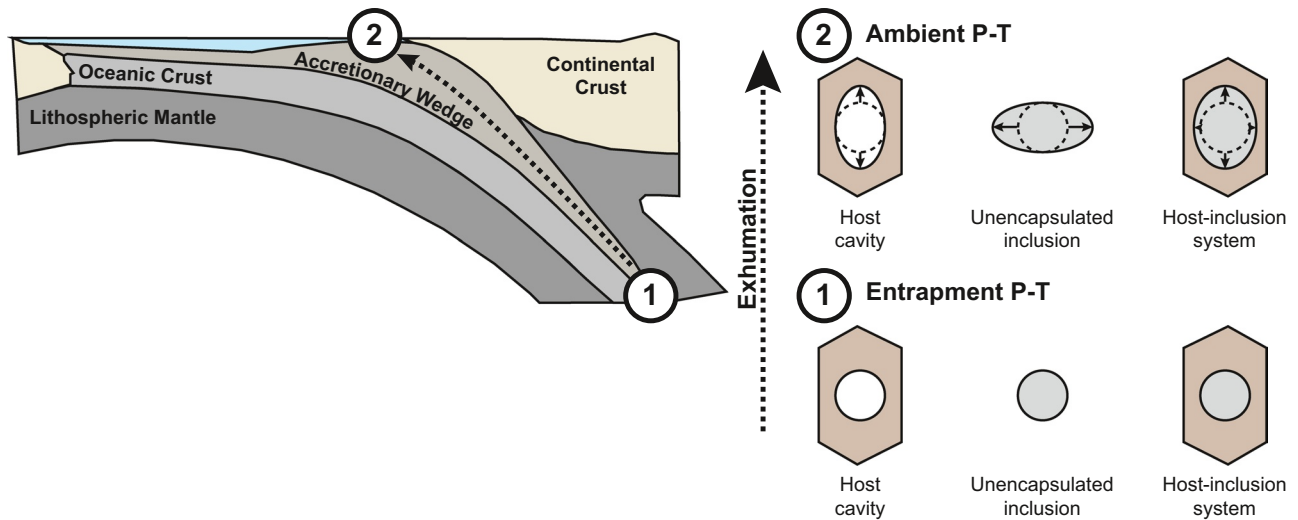


**Figure 1.** Schematic of the change of the volume and shape for an unencapsulated inclusion mineral, the cavity in the host mineral, and the host-inclusion system during exhumation from (1) entrapment conditions within a subduction zone to (2) ambient  $P$ - $T$  conditions.

be hydrostatic, upon exhumation, noncubic hosts and their inclusions will both develop anisotropic strains. If the inclusion completely occupies the cavity of the host mineral (assuming there is no fluid film around it; e.g., Nimis et al., 2016) the final strain state of the inclusion will be a combination of the anisotropic behavior of the host, inclusion, and their elastic interaction (Mazzucchelli et al., 2019). This is a complex problem since the elastic interaction between the two anisotropic minerals is affected by their crystallographic symmetry and mutual relative orientation (Nye, 1985). Following the equivalent inclusion problem developed in Eshelby (1957), we first describe separately the behavior of the host and of the inclusion during the exhumation, and then evaluate their orientation-dependent elastic interactions.

### 2.1. Elastic Anisotropy and the Relative Crystallographic Orientation of Host-Inclusion Systems

The elastic interactions between two elastically isotropic minerals (Angel et al., 2014b, 2017b; Guiraud & Powell, 2006; Zhang, 1998) and an elastically anisotropic inclusion contained in an isotropic host (Mazzucchelli et al., 2019; Zhong et al., 2020a) have been evaluated in previous studies. However, the effect of elastic anisotropy of the host mineral has not been previously described. The effects of elastic anisotropy on the behavior of the host-inclusion system can be visualized in a simplified manner by considering the scenario of an elastically anisotropic stiff host with an elastically anisotropic softer inclusion being exhumed within a subduction zone (Figure 1). At the entrapment  $P$ - $T$  conditions (Figure 1, step 1), the host and inclusion are in a state of mechanical equilibrium and the external load is assumed to be hydrostatic, meaning that no deviatoric stresses exist in either host or inclusion. This implies that if the inclusion were to be removed from the host while they are at entrapment conditions, the inclusion would retain its exact shape and volume. Similarly, the empty cavity inside the host would also retain its exact shape and volume. However, during exhumation to ambient  $P$ - $T$  conditions, the external load (i.e.,  $P_{ext}$ ) and temperature change. If both the host and inclusion are elastically anisotropic, both the shape and volume of each will change (e.g., Mazzucchelli et al., 2019). If corresponding free crystals of the host and inclusion were exhumed separately (Figure 1, step 2), the change in shape and volume of the inclusion and the cavity in host will be controlled by the elastic properties along each crystallographic direction in the two crystals. In this example, the elastic stiffness of the inclusion is greater along the vertical axis than the horizontal axis. Therefore, the inclusion will expand more along the horizontal axis during exhumation. The opposite occurs for the host, where the elastic stiffness is the greatest along the horizontal axis, and therefore, the cavity in the host undergoes the greatest expansion along the vertical axis. However, in reality, the inclusion is constrained inside the cavity in the host and cannot expand freely. Therefore, it is not sufficient to calculate their deformation separately, and we must also account for the elastic interaction between the inclusion and the walls of the cavity in the host. The final change in shape (i.e., deformation) and volume during exhumation is the

result of the elastic anisotropy of the inclusion and the host and is dependent upon their relative crystallographic orientation relationships (RCO).

This behavior is substantially different from the case of an isotropic host and inclusion. In fact, when both crystals are elastically isotropic, the respective volumes change during exhumation but the shape remains constant. In this simplest case of isotropic elasticity and a spherical inclusion in an infinite host, the strain and stress in the inclusion are spherically symmetric meaning that they are equal in all directions (Figure 2a), and the RCO does not affect the strain and stress in the inclusion. When an elastically anisotropic inclusion is contained within an elastically isotropic host subjected to hydrostatic stress (Figure 2b), the host imposes isotropic strain on the inclusion from the point of entrapment. Relative to a free crystal at room conditions the imposed strain on the inclusion will, however, be anisotropic, as will be the consequent stress state of the inclusion (see also Mazzucchelli et al. (2019) for a discussion). However, since the deformation of the host is equal in all directions, the anisotropic strains and stresses developed in the inclusion will be equivalent for every RCO. Mazzucchelli et al. (2019) have shown that the RCO of a spherical anisotropic inclusion (such as quartz or zircon) in quasi-isotropic cubic hosts (such as garnet) does not significantly affect the strain state of the inclusion. For example, even considering the anisotropic elasticity of both minerals, the orientation of a spherical quartz inclusion in garnet affects the strain components by  $<10^{-5}$  (Mazzucchelli et al., 2019), a deviation that cannot be resolved by SC-XRD or Raman measurements and would be negligible for thermobarometric purposes.

Here, we consider the case when both the host and the inclusion are significantly elastically anisotropic and noncubic (Figure 2c). In this case, the deformation of a spherical inclusion upon exhumation is dependent on the RCO of the inclusion compared to its host. This is also illustrated in Figure 1, step 2, because if either the host or inclusion were to be rotated, the resulting volume and shape of the inclusion and host cavity would change. To extend elastic models to elastically anisotropic host and inclusion minerals, the magnitude of the effects of the RCO of the host and inclusion must be known. For example, multiple inclusions with different orientations within the same host mineral would yield different residual strains and stresses. Interpreting these strains and stresses without accounting for the RCO could ultimately translate into incorrectly calculated entrapment conditions or the wrong conclusions regarding the stress state of the inclusion.

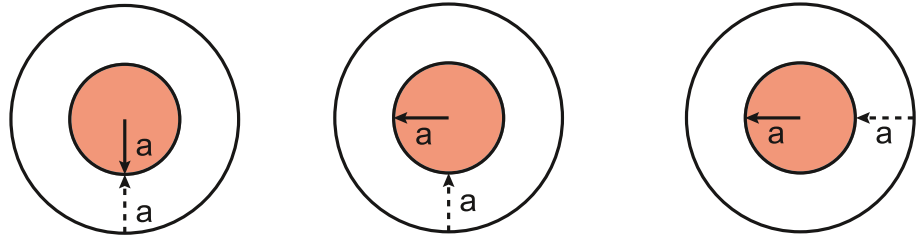
### 3. Calculation of Residual Strain

The calculation of the residual strain, stress and pressure ( $P_{inc}$ ) in the inclusion is divided into two steps: (a) the calculation of the deformation of the host and inclusion from entrapment to room  $P$ - $T$  conditions and then (b) the mutual elastic interaction (elastic relaxation) of the host and inclusion. Because the host and inclusion are elastically anisotropic, their elastic response will be direction-dependent, even if the external stress is lithostatic. Therefore, to compute the deformation of the inclusion, we must account for the RCO between host and inclusion, which can be easily obtained by maintaining the orientation of one of the minerals (i.e., in this case the host), while changing the orientation of the other mineral (i.e., rotating the inclusion). The relative orientation is then represented by a  $3 \times 3$  orientation matrix ( $\mathbf{U}$ ; see Appendix A; Nye, 1985).

In the first step of the calculation, we assume the starting entrapment conditions ( $P_{trap}$ ,  $T_{trap}$ ) and then calculate the deformation of the host during the exhumation from entrapment to ambient conditions. This deformation corresponds to a change in the lattice parameters of the host from the initial (entrapment) to the final (ambient) conditions, which can be calculated from its axial equations of state (see Appendix A). The deformation is then represented by the deformation gradient tensor ( $\mathbf{F}$ ) that can be calculated (e.g., Schlenker et al., 1978) from the change in the lattice parameters. We use the deformation gradient tensor instead of a strain tensor because strain tensors are, by definition, symmetric and exclude rotations such as those arising from the change in unit-cell angles in monoclinic and triclinic crystals. The deformation gradient tensor preserves the information about these rotations, and any strain tensor (e.g., Eulerian or Lagrangian, finite or infinitesimal) can be obtained directly from it (e.g., Schlenker et al., 1978). The deformation of the inclusion encapsulated in the host, is then obtained by transforming the deformation gradient tensor of the host from the reference system of the host to that of the inclusion. From the deformation tensor the lattice parameters and the unrelaxed strain of the inclusion can be found (Data Set S1). The stress

**A. Elastically isotropic host / Elastically isotropic inclusion**

Example: Garnet-in-Diamond



$\sigma_a = \sigma_a = \sigma_a$   $\sigma_{\text{host}}$  is hydrostatic

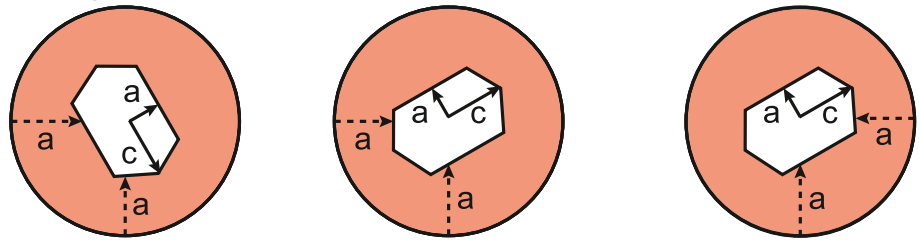
$\epsilon_a = \epsilon_a = \epsilon_a$   $\epsilon_{\text{inc}}$  is isotropic

$\sigma_a = \sigma_a = \sigma_a$   $\sigma_{\text{inc}}$  is hydrostatic

Stress and strains on inclusion do not depend on RCOs

**B. Elastically isotropic host / Elastically anisotropic inclusion**

Example: Quartz-in-Garnet



$\sigma_a = \sigma_a = \sigma_a$   $\sigma_{\text{host}}$  is hydrostatic

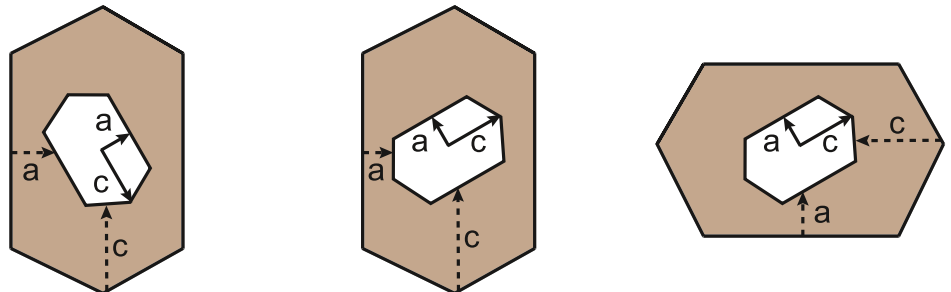
$\epsilon_a = \epsilon_a \neq \epsilon_c$   $\epsilon_{\text{inc}}$  is anisotropic

$\sigma_a = \sigma_a \neq \sigma_c$   $\sigma_{\text{inc}}$  is not hydrostatic

Stress and strains on inclusion do not depend on RCOs

**C. Elastically anisotropic host / Elastically anisotropic inclusion**

Example: Quartz-in-Zircon



$\sigma_a = \sigma_b = \sigma_c$   $\sigma_{\text{host}}$  is hydrostatic

$\epsilon_a \neq \epsilon_b \neq \epsilon_c$   $\epsilon_{\text{inc}}$  is anisotropic

$\sigma_a \neq \sigma_b \neq \sigma_c$   $\sigma_{\text{inc}}$  is not hydrostatic

Stress and strains on inclusion depend on RCOs

**Figure 2.** The effect of relative crystallographic orientations (RCO) on the stress ( $\sigma$ ) and strain ( $\epsilon$ ) of the crystallographic axes of the inclusion and host minerals. (a) An isotropic host-isotropic inclusion system, where the RCOs do not affect the stress or strain. (b) An isotropic host-anisotropic inclusion system. The strain in the inclusion is (in general) anisotropic, when referred to a free crystal at room conditions. As a consequence, the stress in the inclusion is not hydrostatic but is independent of the RCO. (c) An anisotropic host-anisotropic inclusion system. Each RCO will produce unique anisotropic strains and stresses within the inclusion.

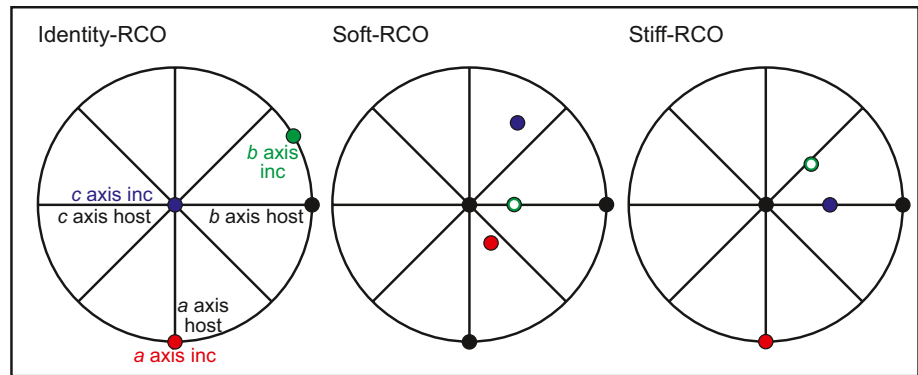


**Figure 3.** Stereographic representations of the investigated relative crystallographic orientations (RCO) of host zircon and quartz inclusions. In each RCO, the host (the black dots) axes are parallel to the Cartesian directions  $x$ ,  $y$ ,  $z$ . Closed symbols indicate that the positive direction of the axis is pointing up and open symbols indicate that the positive direction of the axis is pointing down. Note that the zircon host is not rotated in any of the RCOs. In the identity-RCO, the inclusion has not been rotated and the Cartesian axes of quartz are parallel to those of zircon. The soft-RCO with the quartz inclusion rotated  $-54.09^\circ$  around the  $x$ -axis,  $-54.40^\circ$  around the  $y$ -axis, and  $29.40^\circ$  around the  $z$ -axis to align the softest direction of quartz parallel to the stiffest direction of zircon. The stiff-RCO with the quartz inclusion rotated  $-50.27^\circ$  around the  $x$ -axis to align the stiffest direction of quartz parallel to the stiffest direction of zircon.

state corresponding to this unrelaxed strain is in general nonhydrostatic. However, the mean normal stress ( $\bar{\sigma} = \frac{\sigma_1 + \sigma_2 + \sigma_3}{3}$ ) can be linked to the “thermodynamic pressure” (i.e.,  $-\bar{\sigma} = P_{thermo}$ , where  $P_{thermo}$  is the pressure in an isotropic inclusion embedded in an isotropic host, before accounting for the elastic relaxation) as defined by Angel et al. (2017b). However, this is a virtual state and it is not yet the final strain of the inclusion because we must account for the elastic interaction (i.e., elastic relaxation) of the host and inclusion (e.g., Angel et al., 2014b). In fact, up to this step the deformation of the host is applied to the inclusion as if the host were infinitely rigid. In reality, the inclusion and the host will interact until final mechanical equilibrium is reached (i.e., the stress component normal to the surface of the inclusion is continuous). The elastic relaxation can be calculated applying the relaxation tensor (Mazzucchelli et al., 2019) to the unrelaxed strain obtained from the first part of the calculation. The relaxation tensor was calculated numerically at ambient conditions using the method reported by Mazzucchelli et al. (2019) and Morganti et al. (2020) taking into account the anisotropic elastic properties of the quartz inclusion and the zircon host and their RCO (Data Set S2). By applying the relaxation tensor to the unrelaxed strain, the final residual strain of the inclusion is obtained (Data Set S3), from which, knowing the stiffness tensor of the inclusion, the residual stress in the inclusion can be found. Also in this case, the mean normal stress can be calculated and, as shown by Bonazzi et al. (2019), its negative value can be equated to the residual pressure in the inclusion  $P_{inc}$ . Further details are reported in Appendix A.

#### 4. Evaluation of the Residual Strain and Stress in the Quartz-in-Zircon System

A series of numerical tests were performed to calculate the expected strains and stresses in an elastically isolated quartz inclusion contained in a nonmetamict zircon host for a number of different RCOs. Besides the relevance for several geological applications, the quartz-in-zircon system provides the unique opportunity to evaluate fully anisotropic host-inclusion pairs (Campomenosi et al., 2018; Murri et al., 2018) that have uniaxial crystal symmetries, and relatively simple chemical formulas for which well constrained EoS and room-condition elastic tensors are available (Angel et al., 2017a; Ehlers et al., 2021; Lakshtanov et al., 2007; Özkan et al., 1974). The strain and stress of the quartz inclusion contained in the zircon host were calculated for three RCO's, the identity-RCO, the soft-RCO, and the stiff-RCO (Figure 3). The identity-RCO has no relative rotation of the quartz inclusion or the zircon host, meaning that the  $c$ -axis of both minerals are aligned and the  $a$ - $b$  planes of both minerals are coplanar. The soft-RCO and stiff-RCO were determined by finding the directions corresponding to the greatest and lowest values of the Young's modulus for quartz and zircon and then orienting the quartz inclusion so that the directions with the highest and lowest values

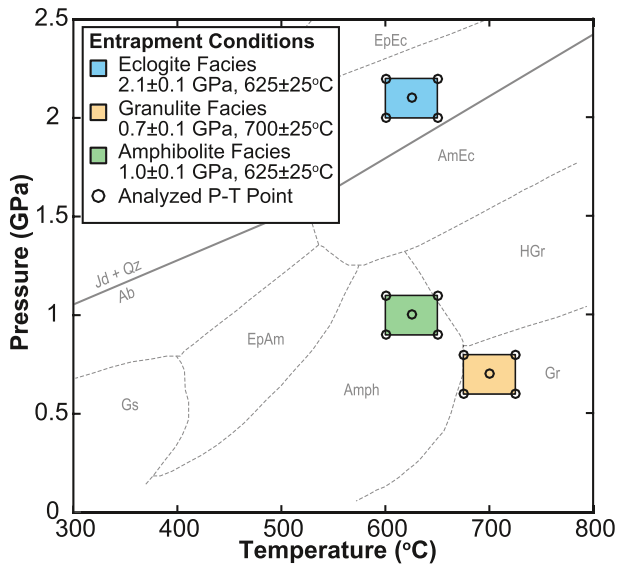


**Figure 4.** The three investigated sets of entrapment conditions. Within each  $P$ - $T$  area, five  $P$ - $T$  points were analyzed, indicated by the open circles.

of the Young's modulus of quartz were parallel to direction of the highest Young's modulus in zircon (see supporting information for further details). Because of the elastic anisotropy of quartz, the directions of the maximum and minimum Young's modulus are not parallel to the unit-cell axes. Since we are only interested in the relative orientations between the host and inclusion, the zircon host was not rotated in any calculation. The transformation matrices corresponding to the three cases are reported in Table S3.

The extension of elastic thermobarometry to anisotropic host-inclusion systems is illustrated through a forward model, in which the strain, stress, and pressure within the inclusion when the host is at room conditions are calculated for predetermined entrapment  $P$ - $T$  conditions. The strains and stresses of a quartz inclusion in the zircon host were determined for three sets of entrapment conditions, each of which contained five individual  $P$ - $T$  points (Figure 4). The strain and stress were calculated for entrapment conditions in the eclogite facies ( $2.1 \pm 0.1$  GPa,  $625^\circ\text{C} \pm 25^\circ\text{C}$ ), amphibolite facies ( $1.0 \pm 0.1$  GPa,  $625^\circ\text{C} \pm 25^\circ\text{C}$ ), and granulite facies ( $0.7 \pm 0.1$  GPa,  $700^\circ\text{C} \pm 25^\circ\text{C}$ ).

The calculation of the host and inclusion deformation from entrapment to room  $P$ - $T$  conditions requires the anisotropic EoS of zircon (Ehlers et al., 2021) and quartz (Angel et al., 2017a) and the orientation matrix to calculate the unrelaxed strains as a function of the entrapment conditions and RCO. The strain in the inclusion, using a free quartz crystal at room conditions ( $10^{-5}$  GPa and  $25^\circ\text{C}$ ) as reference state, was calculated in a new component of the EoSFit7c (Angel et al., 2014a) program, following the procedure outlined in Appendix A.

For each of the three orientations, the relaxation tensor of the elastically anisotropic quartz inclusion and elastically anisotropic zircon host was calculated numerically following the procedure of Mazzucchelli et al. (2019) and Morganti et al. (2020) (Data Set S2). The relaxed strain within the quartz inclusion was obtained from the orientation-specific relaxation tensor and the unrelaxed strain. The stress within the inclusion was then calculated using the elastic tensor of quartz (Lakshtanov et al., 2007; see supporting information for further details), and the volume strain EoS method (e.g., Bonazzi et al., 2019).

The residual pressure and volume strain in the inclusion were also calculated with the simple isotropic model of Angel et al. (2017b) for the same set of entrapment conditions to give a direct comparison of the results from the anisotropic and the isotropic models.

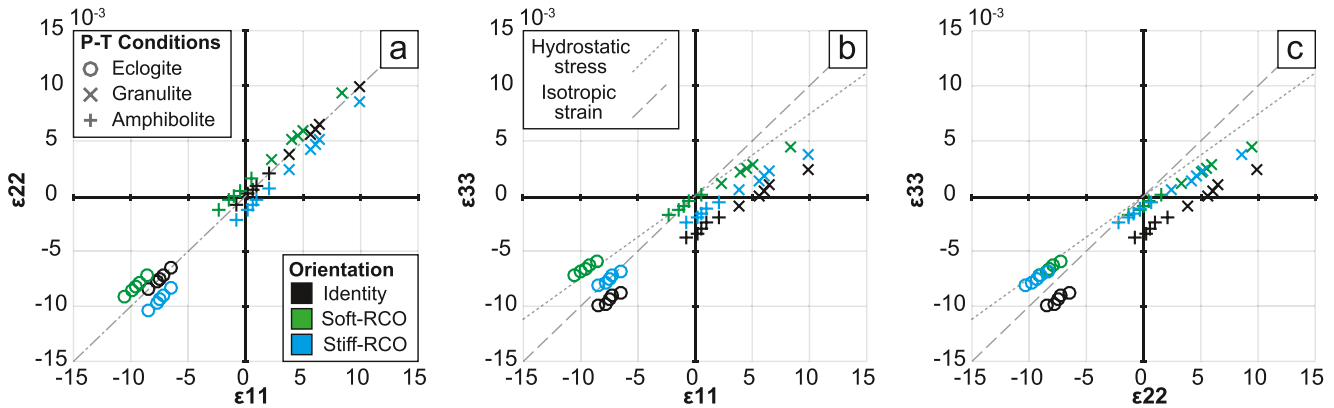
## 5. Results and Discussion

### 5.1. Strain State of the Inclusion

The values of the normal and shear components of the residual strain were calculated for each set of entrapment conditions and RCO (Figure 5, Data Set S1). For each set of entrapment conditions, the unrelaxed strains for the identity-RCO have three normal strains and no shear strains. Shear strains develop as a result of the elastic anisotropy when the inclusion is rotated with respect to the host. Since the stiff-RCO is obtained from the identity orientation by rotating the inclusion around its Cartesian  $x$ -axis, shear strains develop in the  $y$ - $z$  plane (i.e.,  $\epsilon_{23} \neq 0$ ), as expected. On the other hand, the soft-RCO is obtained by subsequent rotation of the inclusion around all three Cartesian axes, and, as a consequence shear strains are developed in all planes (i.e.,  $\epsilon_{23}$ ,  $\epsilon_{13}$ , and  $\epsilon_{12} \neq 0$ ).

The strain results show that each set of entrapment conditions and RCO produces different anisotropic strains in the quartz inclusion. The magnitude of the developed shear strains is dependent on the  $P$ - $T$  of entrapment and the RCO, and range from  $7.86e^{-4}$  to  $2.53e^{-3}$ . Figure 5 shows that the normal strains do not plot along the lines that define the strain state of an inclusion that is subject either to hydrostatic stress or isotropic strain. This shows that anisotropic strains are developed in the inclusion simply because of the

Unrelaxed strains



Relaxed strains

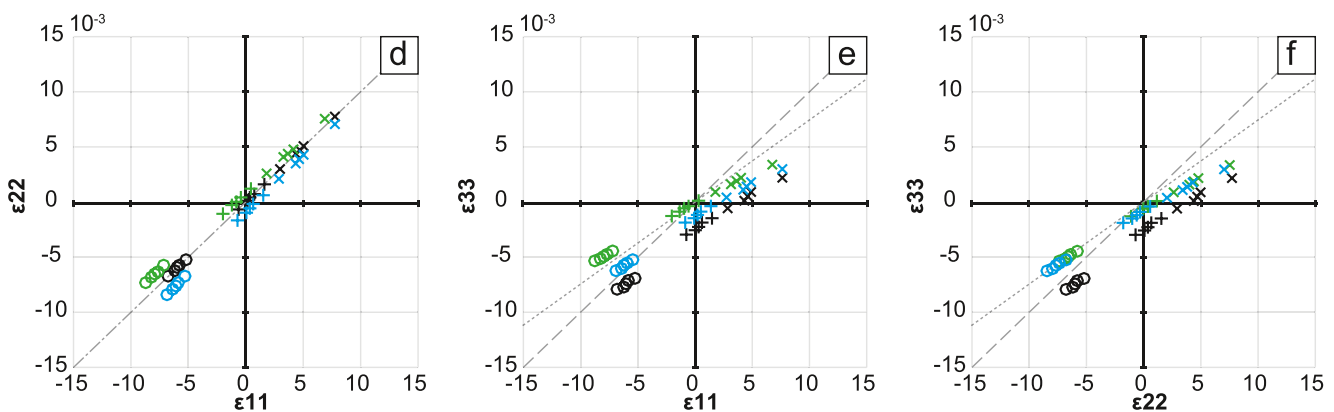


**Figure 5.** Plots of the relaxed anisotropic linear strains ( $\epsilon_{11}$ ,  $\epsilon_{22}$ , and  $\epsilon_{33}$ ) within quartz inclusions contained in the zircon hosts for multiple sets of entrapment conditions and crystallographic orientations (RCO). Within each set of entrapment conditions, the strains of five  $P$ - $T$  points were calculated. The dashed gray lines represent the strains calculated from hydrostatic conditions and isotropic strains.

elastic anisotropy and the RCO. Only for the case of the identity-RCO do the strain components  $\epsilon_{11}$  and  $\epsilon_{22}$  (i.e., those in the  $a$ - $b$  plane) plot along the line of isotropic strain and hydrostatic stress (Figure 5a). This is because the stress applied to the host is hydrostatic and therefore the strain in the  $a$ - $b$  plane of zircon is isotropic, because of its tetragonal symmetry. With the identity-COR, the Cartesian  $x$  and  $y$  axes of the host and inclusion are aligned, and therefore the resulting strain state imposed on the  $a$ - $b$  plane of quartz is also isotropic. However, even with this orientation, the component  $\epsilon_{33}$  is different from the  $\epsilon_{11}$  and  $\epsilon_{22}$ , and therefore the strain state of the inclusion is not isotropic. As a consequence, neither the variation of  $\epsilon_{11}$  with  $\epsilon_{33}$  (Figure 5b) nor that of  $\epsilon_{22}$  with  $\epsilon_{33}$  (Figure 5c) follow the trends that would result from hydrostatic stress or isotropic strain. Also the variation of  $\epsilon_{11}$  with  $\epsilon_{22}$  (Figure 5a) is not isotropic when the inclusion is rotated in the host. This result alone demonstrates that the inclusion can undergo symmetry breaking simply as a consequence of the elastic anisotropy of the host and inclusion minerals and their RCO. The variation of the normal strain components also shows that the residual strain of an anisotropic inclusion contained in an anisotropic host is not isotropic, and therefore, this strain state cannot be predicted by simple isotropic models. Furthermore, the calculated residual strains show that the quartz inclusion is subjected to strains that do not correspond with those predicted from application of a hydrostatic stress. These results are in agreement with the conclusions of Gilio et al. (2021), which show that natural quartz inclusions are not subjected to the strains that correspond to hydrostatic pressure, which means that hydrostatic calibrations of Raman band shifts with pressure should not be used to estimate the residual strain or  $P_{inc}$ .

The volume strain ( $\epsilon_v = \epsilon_{11} + \epsilon_{22} + \epsilon_{33}$ ) was calculated for both the unrelaxed and relaxed strains and indicates the total change in volume of the inclusion versus the same unencapsulated mineral (Figures 6a–6c).



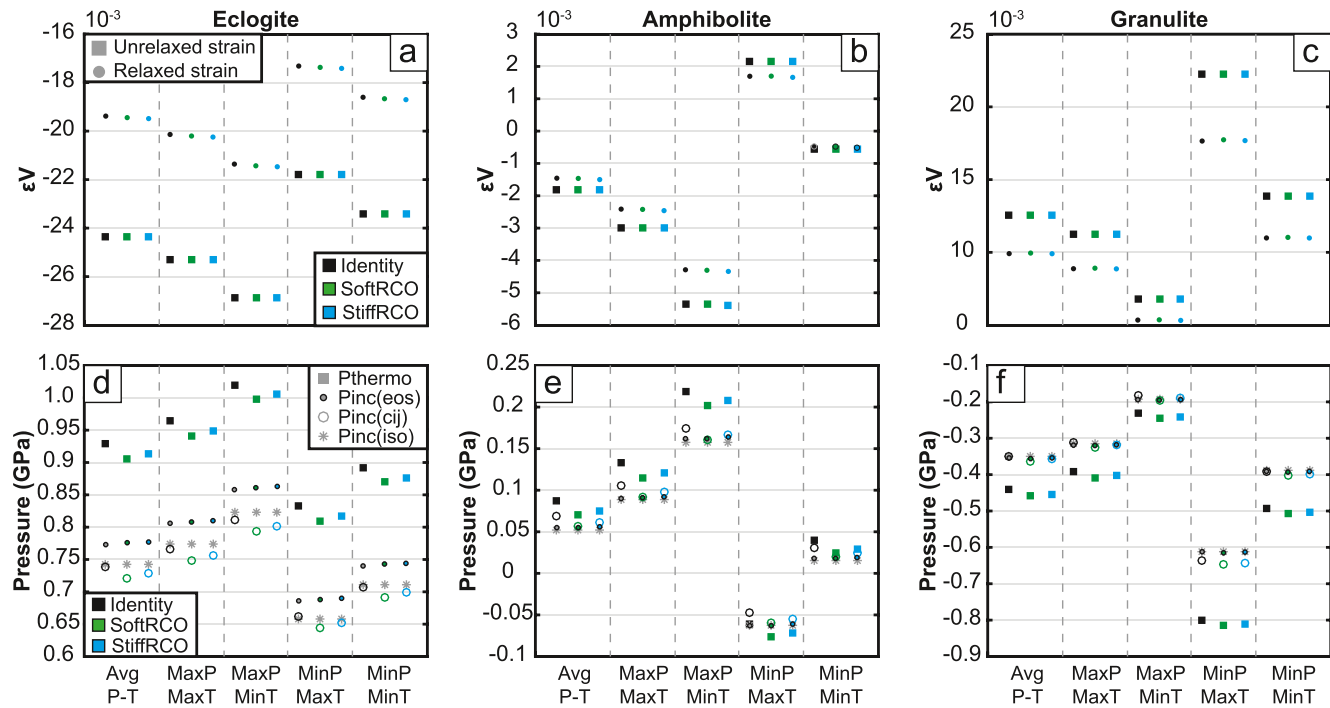


**Figure 6.** Plots of the volume strain ( $\epsilon_v$ ) and inclusion pressure data. The top row shows the volume strain data when the host is at room  $P$ - $T$  conditions. The unrelaxed and relaxed volume strains were plotted for each individual  $P$ - $T$  point and the RCO is indicated by the color of the points. The second row shows the pressure data at room  $P$ - $T$  conditions. The  $(P_{inc}^{cij})$ ,  $(P_{inc}^{eos})$ ,  $(P_{inc}^{cij})$ , and  $(P_{inc}^{iso})$  values were plotted for each individual  $P$ - $T$  point. Note that the  $P_{inc}^{eos}$  and  $P_{inc}^{iso}$  values do not follow the color scheme for easier visibility.

The sign of the  $\epsilon_v$  indicates when the strains are compressive (negative) or tensile (positive). In general, the  $\epsilon_v$  are nearly identical between the different RCOs for each  $P$ - $T$  point. The mutual elastic relaxation ( $\Delta\epsilon_v = \epsilon_v^{unrelax} - \epsilon_v^{relax}$ ) is calculated from the data in Figures 6a–6c and varies as a function of the entrapment conditions such that an inclusion with a greater  $\epsilon_v$  will also undergo greater mutual elastic relaxation.

To show the effect of the inclusion orientation on the  $\epsilon_v$ , the difference between the  $\epsilon_v$  from the rotated RCOs (i.e., the soft-RCO and stiff-RCO) and the identity-RCO were calculated ( $\Delta\epsilon_{v,ori}$ ; Figure 7a). Despite the variation in the normal strain values from the different RCOs, the  $\Delta\epsilon_{v,ori}$  from the unrelaxed strains in rotated orientations yield small differences of  $10^{-6}$ – $10^{-5}$  that are within the numerical precision of our calculations (i.e.,  $\sim 10^{-5}$  on volume strain). These results show that, while the RCO significantly affects the individual unrelaxed strain components (Figure 5), it does not significantly affect the unrelaxed  $\epsilon_v$  of the quartz inclusion contained in the zircon host (Figure 7a). This is expected because the volume strain is an invariant of the deformation gradient tensor for any orientation of the local reference system of the inclusion (see Equation A5). In other words, at this stage the volume change of the inclusion is imposed by the cavity (i.e., the host), and thus it is not affected by the orientation of the inclusion within the cavity. Instead the data in Figure 7a show that the  $\Delta\epsilon_{v,ori}$  from the relaxed strains are in the order of  $10^{-5}$ – $10^{-4}$ . Therefore, the RCO combined with the elastic anisotropy of the two minerals can affect the relaxed  $\epsilon_v$ .

## 5.2. Remnant Stresses

The pressure in the quartz inclusions at room temperature was calculated from both the unrelaxed and relaxed strains. The pressure calculated from the unrelaxed volume strains gives the virtual stress state  $P_{thermo}$  (Angel et al., 2015; Mazzucchelli et al., 2018), which is the calculated pressure in the inclusion without mutual relaxation of the host and inclusion. The  $P_{thermo}$  is calculated as

$$P_{thermo} = -(\sigma_{11} + \sigma_{22} + \sigma_{33})/3$$

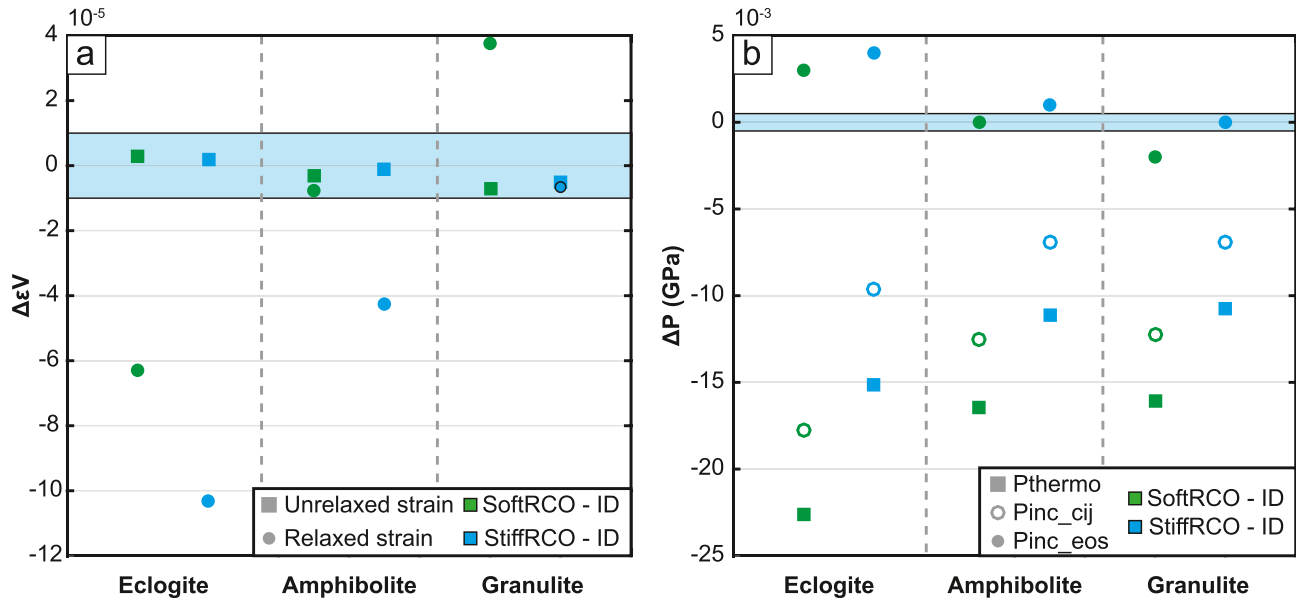


**Figure 7.** Plots showing the effect of RCO on the calculated volume strain and pressure within the inclusion when the host is at room  $P$ - $T$  conditions. The effect of RCO is calculated by taking the respective value of the RCO and subtracting the same respective value of the identity-RCO. Only the data from the average  $P$ - $T$  points are plotted. The blue shaded areas represent the largest numerical uncertainties of our calculations for the volume strain and remnant pressure in the inclusion, (a) Plot of the difference in the unrelaxed and relaxed strain that results from the change in RCO. (b) Plot of the difference in ( $P_{inc}^{cij}$ ), ( $P_{inc}^{eos}$ ), and ( $P_{inc}^{eos}$ ) which vary with RCO.

where  $\sigma$  is the unrelaxed stress calculated as

$$\sigma_{unrelax} = \mathbf{C} \varepsilon_{unrelax}$$

where  $\mathbf{C}$  is the elastic stiffness matrix and  $\varepsilon_{unrelax}$  is the strain in the inclusion before the relaxation. On the other hand, the final pressure on the inclusion at room temperature conditions ( $P_{inc}$ ) is calculated from the relaxed volume strains and accounts for mutual elastic relaxation.  $P_{inc}$  was calculated using three different models (e.g., Bonazzi et al., 2019). The elastic tensor method gives an inclusion pressure

$$P_{inc}^{cij} = -(\sigma_{11} + \sigma_{22} + \sigma_{33})/3$$

where  $\sigma$  is the relaxed stress calculated as

$$\sigma_{relax} = \mathbf{C} \varepsilon_{relax}$$

where  $\mathbf{C}$  is the elastic stiffness matrix of the inclusion and  $\varepsilon_{relax}$  is the residual strain in the inclusion. The inclusion volume EoS method ( $P_{inc}^{eos}$ ) was calculated as

$$P_{inc}^{eos} = E \Delta S(\varepsilon_v)$$

by applying the volumetric EoS of the inclusion phase to the volume strain of the inclusion (e.g., Bonazzi et al., 2019). Lastly, the residual pressure was also obtained from the isotropic model that assumes isotropic properties for the host and the inclusion ( $P_{inc}^{iso}$ ; e.g., Angel et al., 2017b), and is therefore unaffected by the RCO.

For the eclogite facies tests,  $P_{inc}^{cij}$  of 0.642–0.811 GPa and  $P_{inc}^{eos}$  of 0.686–0.858 GPa are obtained and indicate that the inclusions are under compressive stress. For this set of entrapment conditions, the  $P_{inc}^{eos}$  is greater than the  $P_{inc}^{cij}$  and  $P_{inc}^{iso}$  for each  $P$ - $T$  point (Figure 6d). This pattern arises because, in the range of

residual strains investigated here, the EoS does not account for the decrease in bulk modulus due to the deviatoric strain state of the inclusion, while the constant stiffness tensor does not account for the stiffening of the structure with stress. The combined effect leads to a  $P_{inc}^{eos}$  greater than the  $P_{inc}^{cij}$ , as reported by Bonazzi et al. (2019). The  $P_{inc}^{iso}$  is slightly greater than the  $P_{inc}^{cij}$  for each  $P$ - $T$  point. For a  $P_{inc}^{cij}$  of 0.79 GPa (Figure 6; eclogite facies  $P_{max} - T_{min}$ , soft-RCO), the  $P_{inc}^{cij}$  differs by <0.03 GPa (i.e., the discrepancy is  $\approx 4\%$ ). However, the magnitude of the discrepancy increases as the  $\varepsilon_v$  of the inclusion increases and when the inclusion is rotated.

In the amphibolite facies tests, smaller remnant pressures were obtained that ranged from  $-0.060$  to  $0.174$  GPa for the  $P_{inc}^{cij}$  and  $-0.066$  to  $0.162$  GPa for the  $P_{inc}^{eos}$  (Figure 6e). Because inclusions were “entrapped” near the entrapment isomeke that intersects room  $P$ - $T$  conditions, the amphibolite facies tests yielded both positive and negative  $P_{inc}$  values depending on the specific  $P$ - $T$  point. Therefore, a host-inclusion system exhumed from this range of entrapment conditions would have a slight deformation of the host cavity, explaining why the pressure in the inclusion is approximately zero.

The granulite facies tests yielded negative pressures with a  $P_{inc}^{cij}$  of  $-0.183$  to  $-0.649$  GPa and a  $P_{inc}^{eos}$  of  $-0.194$  to  $-0.616$  GPa, indicating that the quartz inclusions are calculated to be under tensile stress in the zircon hosts (Figure 6f). In each of the tests, the  $P_{inc}$  values from each of the different models are almost the same. However, for the largest tensile stress inclusions (i.e., those entrapped at the  $P_{min} - T_{max}$  point), the  $P_{inc}^{cij}$  yields an average stress  $-0.04$  GPa (more tensile) greater in magnitude than the  $P_{inc}^{eos}$  and  $P_{inc}^{iso}$  models.

## 6. Implications

### 6.1. Elastic Deformation in Anisotropic Host-Inclusion Systems

We have shown how the deformation in the host and the inclusion from entrapment to room  $P$ - $T$  conditions can be calculated accounting for the full anisotropy of the minerals and their RCO. The models are based on the use of the volumetric and axial EoS for the host and the inclusion to evaluate how their lattice parameters change with the change of the external  $P$  and  $T$  during exhumation. The relaxation tensor (Mazzucchelli et al., 2019; Morganti et al., 2020) is then used to account for the anisotropic elastic interaction between the host and the inclusion and determine residual strains and stresses in the inclusion. This approach can be applied to host-inclusion systems with well-known volume and axial EoS and stiffness tensors which are measured on the exact composition of the mineral, such as rutile, zircon, quartz, mantle olivine, etc., provided that the RCO is known. Our results from the anisotropic quartz-in-zircon model show that the individual components of the strain developed in the inclusion during exhumation are a function of the entrapment conditions and the RCO (Figure 5). The RCO also affects the volume strain and the residual pressure in the inclusion (Figure 7). Despite this effect, for a quartz inclusion in a zircon host, the discrepancy on the  $P_{inc}$  due to the RCOs considered in this study is <0.06 GPa. However, this cannot be assumed as a general limit and the effect of RCO on the strain, stress, and mean normal stress in the inclusion should be evaluated explicitly on a case-by-case basis.

Previous studies of elastically anisotropic mineral inclusions in natural samples have used SC-XRD (e.g., Alvaro et al., 2020) and Raman spectroscopy (Murri et al., 2018) to determine the strain state of the inclusion while it is still fully entrapped in the host. SC-XRD has the advantage to provide simultaneously the RCO and the average strain state of an inclusion still entrapped within its host. Therefore, each component of the strain of the inclusion, and not just the volume strain, can be measured with SC-XRD. However, SC-XRD only provides the average strain state over the entire volume probed by the X-ray beam, thus averaging out strain inhomogeneities due to the geometry of the inclusion. Nonetheless, our results show that the volume strains of the quartz inclusions at room temperature conditions are greater than 0.0018 which is an order of magnitude larger than the instrumental precision of XRD diffractometers. Therefore, in principle, SC-XRD can be used to determine the volume strain of quartz inclusions in zircon entrapped at these metamorphic conditions.

Confocal Raman spectroscopy on the other hand, offers submicrometric spatial resolution, faster analytical times, and is commonly available in many laboratories (e.g., Korsakov et al., 2020). However, calculation of the strains from the measured Raman shifts relies on the knowledge of the phonon-mode Grüneisen

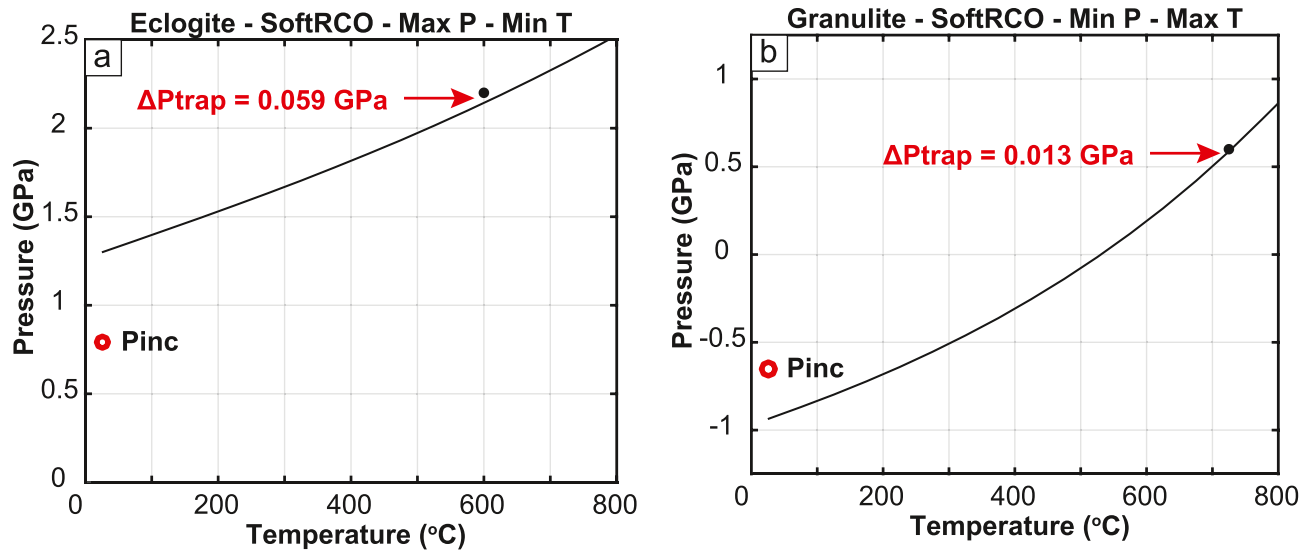


**Figure 8.** The discrepancies on calculated entrapment conditions that result from the application of isotropic elastic models to determine the entrapment conditions of an anisotropic inclusion in an anisotropic host. The two simulations that gave the largest discrepancy between the ( $P_{inc}^{cij}$ ) and the ( $P_{inc}^{iso}$ ) are shown. The black lines are the calculated entrapment isomekes, the red circle is ( $P_{inc}^{cij}$ ), and the black dots are the original “entrapment” conditions.

tensors of the mineral (e.g., Angel et al., 2019; Murri et al., 2018). As shown in Figure 5, when an elastically anisotropic inclusion is not aligned with the elastically anisotropic host, the strain components  $\varepsilon_{11}$  and  $\varepsilon_{22}$  are not equivalent and shear strains develop, implying that there is breaking of the uniaxial symmetry in the inclusion. Such symmetry breaking of the inclusion crystal must also affect the values of the components of the phonon-mode Grüneisen tensors which determine the Raman shifts which arise from the strains applied to the inclusions. Recent Density Functional Theory (DFT) calculations of the phonon-mode Grüneisen tensors of quartz (Murri et al., 2018) explicitly assume that the symmetry of the crystal is preserved. Therefore, they cannot be applied to strain states where the  $\varepsilon_{11}$  component is different from  $\varepsilon_{22}$ , or those with nonzero shear components. The magnitude of the effect of symmetry breaking on the phonon-mode Grüneisen tensors of minerals has not yet been calculated in DFT simulations. The experiments of Briggs and Ramdas (1977) on quartz under nonhydrostatic stress suggest that this effect can be significant compared to the shifts without symmetry breaking. However, due to the small range of compression and the experimental uncertainties, the results are not conclusive. The quantification of the effect of symmetry breaking on the phonon-mode Grüneisen tensors will require investigation with *ab initio* calculations (e.g., Murri et al., 2018) supported by synthesis experiments at known entrapment conditions (e.g., Bonazzi et al., 2019; Thomas & Spear, 2018).

## 6.2. Benefits of an Anisotropic Elastic Model

By using the anisotropic model, we have introduced a procedure to evaluate the extent to which simple models for elastic barometry based on elastic isotropy can be applied to anisotropic host-inclusion systems and their resulting errors. To this aim, the residual strain and stress calculated in the inclusion using the anisotropic model can be used to back-calculate the entrapment conditions with the isotropic model. First the  $P_{inc}^{cij}$  is calculated from the mean normal stress in the inclusion, and then is used as the input to calculate the entrapment isomeke (Angel et al., 2017b). Since the calculation of the entrapment isomeke assumes elastically isotropic behavior, a discrepancy between the original entrapment conditions and the isomeke is expected. For the case of a quartz inclusion in a zircon host, the entrapment isomeke can be calculated by using the volumetric EoS of Angel et al. (2017a) and Ehlers et al. (2021). The resulting isomekes are relatively flat in  $P$ - $T$  space, suggesting that the quartz-in-zircon system is best used as a barometer (Figure 8). Each of the calculated isomekes nearly intersects the original conditions of the quartz inclusion “entrap-

ment,” suggesting that the quartz-in-zircon isotropic elastic model is suitable for calculating the entrapment conditions.

As shown above, this procedure can be extended to other host-inclusion systems to permit estimation of the errors that result from the application of simple isotropic models to anisotropic host-inclusions systems with low symmetry, which could not previously be evaluated (Cisneros et al., 2020; Guo et al., 2021; Taguchi et al., 2019). It should be noted that our calculations assume a spherical inclusion in a practically infinite host. A different geometry of the system (e.g., a nonspherical inclusion, or an inclusion close to the free surface of the host) would affect the individual components of the strain state of the inclusion, and also its residual pressure and volume strain. For irregular shapes, the effect of the geometry on the residual volume strain could become relevant (e.g., flat inclusions, see Mazzucchelli et al., 2018) and should be taken into account in elastic thermobarometry calculations. Therefore, we suggest that the combined effect of the geometry, orientation, and the elastic anisotropy on the individual components of the strain should be evaluated on a case-by-case basis.

The anisotropic model can, in principle, be inverted to calculate directly the  $P$ - $T$  conditions of entrapment of an inclusion from a single measurement of its residual strain. When the residual pressure, or the volume strain, of the inclusion (i.e., a single scalar) is measured in the inclusion and is used together with an isotropic elastic model to estimate the entrapment conditions, it is only possible to determine a single univariant curve of possible entrapment (or equilibration) conditions. But the determination of the single point on that curve requires an additional constraint on the temperature or pressure of the entrapment or equilibration. On the other hand, Alvaro et al. (2020) have shown that by measuring at least two strain components in the same inclusion, and accounting for their anisotropic behavior, unique  $P$ - $T$  conditions of elastic equilibration of the inclusion within the host can be determined in certain circumstances. Therefore, each individual elastically anisotropic inclusion is capable of providing multiple independent thermobarometric constraints. To achieve this, however, the residual strain state of the inclusion must be measured accurately (Alvaro et al., 2020).

### 6.3. The Quartz-in-Zircon System

Zircon is a common accessory mineral in many bulk rock compositions that has been used extensively for geochronology (e.g., Schoene, 2013) and trace element thermometry (e.g., Watson & Harrison, 2005). During crystallization, zircon frequently entraps mineral inclusions and, because it is physically and chemically resistant to alteration, zircon can preserve these inclusions during metamorphic evolution (e.g., Bell et al., 2015). These properties along with the well-known EoS for zircon, relatively high crystal symmetry, and simple chemical structure, make zircon suitable for elastic thermobarometry. However, while previous studies were restricted to the use of zircon as an inclusion in other cubic and nearly elastically isotropic host minerals (e.g., Baldwin et al., 2021; Zhong et al., 2019), our results accounting for its elastic anisotropy open the way to using zircon as a host mineral.

However, there are practical considerations that need to be taken into account prior to the application of quartz-in-zircon elastic thermobarometry, such as the elastic isolation of quartz inclusions, the influence of trace elements and chemical zoning in zircon, metamictization, and the structural differences of zircon crystallized from different geologic settings (i.e., metamorphic (re)crystallization versus magmatic crystallization). The effect of elastic isolation and inclusion/host grain size has been investigated numerically (Mazzucchelli et al., 2018; Zhong et al., 2018) and experimentally (Campomenosi et al., 2018), and these studies have concluded that inclusions must be located  $>3$  inclusion radii within the host to preserve their original elastic strains. Recently, Campomenosi et al. (2020) evaluated many of these other factors and proposed a detailed protocol to determine whether a zircon inclusion is suitable for elastic thermobarometry, and many of these same criteria can be used to determine if a zircon host with quartz inclusions is suitable for elastic modeling. Their results suggest that if the Raman spectra of a zircon host is measured at ambient conditions, a variation in frequency and broadening of the main peaks with respect to a reference crystal could result from the incorporation of nonformula elements (e.g., U, Hf) or a significant degree of metamictization. In both cases, the elastic properties of the zircon might change with respect to those of a pure nonmetamict zircon, and therefore should be taken into account when selecting zircon hosts for elastic

thermobarometric calculations. Therefore, if a significant change in Raman peak positions with respect to the reference crystal or broadening of the peaks are detected in the zircon host, the sample is probably not suitable for elastic thermobarometry unless the appropriate EoS is known. Campomenosi et al. (2020) also found that there are no discernable differences in the Raman spectra of magmatic and metamorphic zircon, implying that zircon crystals from either environment can be used for elastic modeling. Prior to interpreting the geologic significance of quartz-in-zircon remnant pressures, it is important to consider the potential effects of the crystallization environment on the strains and stresses preserved in the quartz inclusion. For example, the strains of quartz inclusions in zircon crystals that formed in magmatic settings or experienced reheating events may not reflect the original conditions of inclusion entrapment during zircon crystallization, but rather the  $P$ - $T$  conditions of elastic (re)equilibration during cooling (e.g., Baldwin et al., 2021; Moulas et al., 2020; Zhong et al., 2020b). However, this potential complication also provides opportunities for constraining geologic events that may otherwise be overlooked, such as reheating during exhumation (e.g., Baldwin et al., 2021) or overpressurization during continued subduction (e.g., Alvaro et al., 2020).

## 7. Conclusions

We have extended elastic geobarometry to account for the anisotropic elastic properties and RCO of a host-inclusion system where both minerals are noncubic using the deformation tensor. This model was used to numerically evaluate the effect of elastic anisotropy and RCO on the strains and stresses developed in an elastically anisotropic quartz inclusion entrapped in an elastically anisotropic zircon host after “exhumation” from various sets of entrapment conditions. We conclude that the anisotropic quartz-in-zircon elastic model is suitable for elastic thermobarometry and that the near ubiquity of zircon as an accessory mineral in crustal rocks implies that the quartz-in-zircon elastic model will be widely applicable. Furthermore, thermobarometric results from the quartz-in-zircon elastic model can be integrated with zircon geochronology and trace element thermometry models to further decipher the temporal and spatial scales of crustal processes.

## Appendix A

The objective of this appendix is to provide a detailed and generalized explanation of the inputs, assumptions, and calculations implemented in the anisotropic elastic model. Note that while we have discussed our analysis in terms of the final conditions ( $P_{end}, T_{end}$ ) being at room conditions, the analysis applies equally well to any other external conditions, allowing the strain state of the inclusion to be calculated along its entire exhumation path. The following calculations rely on these fundamental assumptions:

- The external load on the host at ( $P_{trap}, T_{trap}$ ) and ( $P_{end}, T_{end}$ ) is hydrostatic
- The deformation of both minerals is purely elastic
- The host is taken as the global reference system

### A1. Axial Conventions and Relative Orientations

We denote the natural basis of the crystal as  $Z = \{\mathbf{a}, \mathbf{b}, \mathbf{c}\}$ , where  $\mathbf{a}, \mathbf{b}, \mathbf{c}$  are the lattice vectors of the crystal. The components of the tensors that represent the physical properties of crystals (e.g., the elastic tensor) are defined with respect to a Cartesian coordinate system attached to the crystallographic axes. We define the Cartesian basis as  $C = \{\mathbf{i}, \mathbf{j}, \mathbf{k}\}$ . The orientation of the crystallographic coordinate system relative to the Cartesian coordinate system is fixed by means of an axial convention.  $A$  is the matrix that represents the transformation of the unit cell onto a Cartesian reference basis (Equation S1). Therefore, given the position  $X_Z$  of a point in the crystal basis, the corresponding coordinates in the Cartesian basis are given by  $X_C = AX_Z$ . The metric tensor  $G$  of a crystal is obtained as  $G = A^T A$  (e.g., Busing & Levy, 1967; Schlenker et al., 1978). For each mineral, we follow the axial convention that was assumed for the experimental determination of its stiffness tensor  $C$  and it is maintained for all of the calculations.

Without any loss of generality, the relative orientation between the host and the inclusion is obtained by keeping the host orientation fixed and defining the Cartesian reference system of the inclusion with respect to that of the unrotated host. The relation between the local reference system of the inclusion and the global reference system of the host is expressed by the transformation matrix  $U$ :

$$U = \begin{pmatrix} \cos(\widehat{x_1^i x_1^h}) & \cos(\widehat{x_1^i x_2^h}) & \cos(\widehat{x_1^i x_3^h}) \\ \cos(\widehat{x_2^i x_1^h}) & \cos(\widehat{x_2^i x_2^h}) & \cos(\widehat{x_2^i x_3^h}) \\ \cos(\widehat{x_3^i x_1^h}) & \cos(\widehat{x_3^i x_2^h}) & \cos(\widehat{x_3^i x_3^h}) \end{pmatrix} \quad (A1)$$

where  $\widehat{x_1^i x_1^h}$  is the angle in radians between the Cartesian axis  $i$  of the inclusion and the axis  $j$  of the host.

## A2. Step 1: Calculation of Unrelaxed Strain in the Inclusion

When a crystal is deformed its particles are displaced relative to each other. We denote the position of a particle before deformation as  $\mathbf{X}$  and the position of the same particle in the deformed configuration as  $\mathbf{x}$ . The second-rank deformation gradient tensor is defined as

$$F_{ij} = \frac{\partial x_i}{\partial X_j} \quad (A2)$$

and the deformation gradient tensor can be obtained as

$$\mathbf{F} = \mathbf{A}_1 \mathbf{A}_0^{-1} \quad (A3)$$

where  $\mathbf{A}_0$  and  $\mathbf{A}_1$  are the transformation matrices of the unit cell onto a Cartesian reference basis, before and after the deformation, respectively (Schlenker et al., 1978). Note that in Schlenker et al. (1978) the transposes of the matrices  $\mathbf{A}_i$  are denoted as  $(\text{mat}_{B_i}^C \ 1)$ .

In this step, we obtain the deformation of the cavity (i.e., the host) developed during exhumation from a given hydrostatic  $P_{trap}, T_{trap}$  to  $P_{end}, T_{end}$ . The unit cell parameters of the host at  $P_{trap}, T_{trap}$  and at  $P_{end}, T_{end}$  are calculated from its volume and axial equations of state. The matrices  $\mathbf{A}_{trap,h}$  (representing the host cell at  $P_{trap}, T_{trap}$ ) and  $\mathbf{A}_{end,h}$  (representing the host cell at  $P_{end}, T_{end}$ ) can be calculated from the unit cell parameters at the two conditions (Equation S1). The deformation gradient tensor of the host ( $\mathbf{F}_h$ ) going from the undeformed to the deformed state is then obtained as

$$\mathbf{F}_h = \mathbf{A}_{end,h} \mathbf{A}_{trap,h}^{-1} \quad (A4)$$

So far Equations A2–A4 have described the deformation of the empty cavity within the host crystal. However, we are interested in calculating the strain of an inclusion forced to the same deformation as the cavity and referred to a free inclusion crystal at  $P_{end}, T_{end}$ .

The unit cell parameters of the inclusion at entrapment can be calculated from its volume and axial EoS (e.g., Alvaro et al., 2020; Angel et al., 2017a) and referred to the Cartesian reference system of the inclusion giving the matrix  $\mathbf{A}_{trap,inc}$  (Equation S1). Since we assume that the deformation of the cavity is completely applied to the inclusion,  $\mathbf{F}_h$  has to be transformed from the Cartesian coordinate system of the host to the local reference system of the inclusion. Therefore, the deformation gradient of the inclusion ( $\mathbf{F}_{inc}$ ) is obtained as

$$\mathbf{F}_{inc} = \mathbf{U} \mathbf{F}_h \mathbf{U}^T \quad (A5)$$

where  $\mathbf{F}_h$  is the deformation gradient tensor of the host and  $\mathbf{U}$  is the transformation matrix between the global (host) and local (inclusion) Cartesian reference systems.

At this stage, the inclusion is in an unrelaxed condition, since it is forced to have the same deformation as the cavity.  $\mathbf{F}_{inc}$ , therefore, represents the deformation gradient of the inclusion referenced to a free inclusion crystal at  $P_{trap}, T_{trap}$  as the undeformed state. The matrix  $\mathbf{A}_{unrelax,inc}$  of the inclusion at this stage ( $P_{thermo}, T_{end}$ ) can then be obtained from the  $\mathbf{A}_{trap,inc}$  matrix calculated at entrapment, as

$$\mathbf{A}_{unrelax,inc} = \mathbf{F}_{inc} \mathbf{A}_{trap,inc} \quad (\text{A6})$$

And the unit cell parameters of the inclusion at this stage are found from the metric tensor ( $\mathbf{G}_{unrelax,inc}$ ) which is found as

$$\mathbf{G}_{unrelax,inc} = \mathbf{A}_{unrelax,inc}^T \mathbf{A}_{unrelax,inc} \quad (\text{A7})$$

However, we prefer to describe the deformation of the inclusion using a free crystal of the same phase at ambient conditions ( $P_{end}, T_{end}$ ) as a reference state, as this is what is used as a reference for inclusion measurements by SC-XRD or Raman in the laboratory. Knowing the EoS of the inclusion phase, we can calculate the unit cell parameters of a free crystal at  $P_{end}, T_{end}$  and obtain the matrix  $\mathbf{A}_{free,inc}$ . We can then calculate the deformation gradient tensor ( $\mathbf{D}_{inc}$ ) of the inclusion referred to a free crystal at ambient conditions as

$$\mathbf{D}_{inc} = \mathbf{A}_{unrelax,inc} \mathbf{A}_{free,inc}^{-1} \quad (\text{A8})$$

Finally, the unrelaxed Lagrangian infinitesimal strain of the inclusion referred to a free crystal at  $P_{end}, T_{end}$  is

$$\boldsymbol{\varepsilon}_{unrelax,inc} = \frac{1}{2} (\mathbf{D}_{inc} + \mathbf{D}_{inc}^T) - \mathbf{I} \quad (\text{A9})$$

where  $\mathbf{I}$  is the second-rank identity matrix.

### A3. Step 2: Elastic Interaction and Calculation of Relaxed Strain in the Inclusion

The final relaxed strain of the inclusion can then be calculated by applying the fourth-rank relaxation tensor (Mazzucchelli et al., 2019; Morganti et al., 2020). For an elastically anisotropic host with an elastically anisotropic inclusion, the relaxation tensor is calculated numerically with Finite Element Modeling (see Morganti et al., 2020 for a complete discussion) and accounts for the shape of the inclusion, the relative orientation, and the anisotropic elastic properties (i.e., the stiffness tensor) of both the host and the inclusion.

Given the specific relaxation tensor for the system, the relaxed strain in the inclusion can be found as

$$\boldsymbol{\varepsilon}_{relax,inc} = \mathbf{R} \boldsymbol{\varepsilon}_{unrelax,inc} \quad (\text{A10})$$

where  $\boldsymbol{\varepsilon}_{rel,inc}$  is the residual strain in the inclusion, referred to the local Cartesian reference system of the inclusion. From  $\boldsymbol{\varepsilon}_{rel,inc}$ , the stress of the inclusion ( $\boldsymbol{\sigma}_{rel,inc}$ ) is obtained as

$$\boldsymbol{\sigma}_{relax,inc} = \mathbf{C} \boldsymbol{\varepsilon}_{relax,inc} \quad (\text{A11})$$

where  $\mathbf{C}$  is the fourth-rank stiffness tensor of the inclusion. The residual pressure in the inclusion is then defined as

$$P_{inc} = - \frac{\text{trace}(\boldsymbol{\sigma}_{relax,inc})}{3} = - \frac{\sigma_{11} + \sigma_{22} + \sigma_{33}}{3} \quad (\text{A12})$$



## Data Availability Statement

The supporting information and all the data sets can be downloaded from <https://doi.org/10.4121/14537856>. These supplementary materials provide further details about the elastic properties, axial conventions, and relative orientations and all the results of the calculations in table format.

## Acknowledgments

This material is based upon work supported by the National Science Foundation under Award No. (1952698) to J. P. Gonzalez, and the European Research Council under the European Union's Horizon 2020 research and innovation program grant agreement 714936 (ERC-STG TRUE DEPTHS) to M. Alvaro. M. Alvaro has been also supported by the Ministero dell'Istruzione dell'Università e della Ricerca (MIUR) Progetti di Ricerca di Interesse Nazionale (PRIN) Bando PRIN 2017-Prot. 2017ZE49E7\_005. Part of the work of MLM was carried out at the Mainz Institute of Multiscale Modeling and supported by this institution and by the Alexander von Humboldt research fellowship. The authors thank two anonymous reviewers for constructive comments. Open access funding enabled and organized by Projekt DEAL.

## References

- Alvaro, M., Mazzucchelli, M. L., Angel, R. J., Murri, M., Campomenosi, N., Scambelluri, M., et al. (2020). Fossil subduction recorded by quartz from the coesite stability field. *Geology*, *48*(1), 24–28. <https://doi.org/10.1130/G46617.1>
- Angel, R. J., Alvaro, M., Miletich, R., & Nestola, F. (2017a). A simple and generalised P–T–V EoS for continuous phase transitions, implemented in EosFit and applied to quartz. *Contributions to Mineralogy and Petrology*, *172*(5), 29. <https://doi.org/10.1007/s00410-017-1349-x>
- Angel, R. J., Gonzalez-Platas, J., & Alvaro, M. (2014a). EosFit7c and a fortran module (library) for equation of state calculations. *Zeitschrift für Kristallographie*, *229*(5), 405–419. <https://doi.org/10.1515/zkri-2013-1711>
- Angel, R. J., Mazzucchelli, M. L., Alvaro, M., & Nestola, F. (2017b). EosFit-Pinc: A simple GUI for host-inclusion elastic thermobarometry. *American Mineralogist*, *102*(9), 1957–1960. <https://doi.org/10.2138/am-2017-6190>
- Angel, R. J., Mazzucchelli, M. L., Alvaro, M., & Nestola, F. (2020). “EosFit-Pinc: A simple GUI for host-inclusion elastic thermobarometry”—Reply to Zhong et al. *American Mineralogist*, *105*(10), 1587–1588. <https://doi.org/10.2138/am-2020-7616CCBY>
- Angel, R. J., Mazzucchelli, M. L., Alvaro, M., Nimis, P., & Nestola, F. (2014b). Geobarometry from host-inclusion systems: The role of elastic relaxation. *American Mineralogist*, *99*(10), 2146–2149. <https://doi.org/10.2138/am-2014-5047>
- Angel, R. J., Murri, M., Mihailova, B., & Alvaro, M. (2019). Stress, strain and Raman shifts. *Zeitschrift für Kristallographie*, *234*(2), 129–140. <https://doi.org/10.1515/zkri-2018-2112>
- Angel, R. J., Nimis, P., Mazzucchelli, M. L., Alvaro, M., & Nestola, F. (2015). How large are departures from lithostatic pressure? Constraints from host-inclusion elasticity. *Journal of Metamorphic Geology*, *33*(8), 801–813. <https://doi.org/10.1111/jmg.12138>
- Ashley, K. T., Caddick, M. J., Steele-MacInnis, M. J., Bodnar, R. J., & Dragovic, B. (2014). Geothermobarometric history of subduction recorded by quartz inclusions in garnet. *Geochemistry, Geophysics, Geosystems*, *15*, 350–360. <https://doi.org/10.1002/2013GC005106>
- Baldwin, S. L., Schönig, J., Gonzalez, J. P., Davies, H., & Eynatten, H. V. (2021). Garnet sand reveals rock recycling processes in the youngest exhumed high- and ultrahigh-pressure terrane on earth. *Proceedings of the National Academy of Sciences of the United States of America*, *118*(3), e2017231118. <https://doi.org/10.1073/pnas.2017231118>
- Bell, E. A., Boehnke, P., Hopkins-Wielicki, M. D., & Harrison, T. M. (2015). Distinguishing primary and secondary inclusion assemblages in jack hills zircons. *Lithos*, *234–235*, 15–26. <https://doi.org/10.1016/j.lithos.2015.07.014>
- Bonazzi, M., Tumiati, S., Thomas, J. B., Angel, R. J., & Alvaro, M. (2019). Assessment of the reliability of elastic geobarometry with quartz inclusions. *Lithos*, *350–351*, 105201. <https://doi.org/10.1016/j.lithos.2019.105201>
- Briggs, R. J., & Ramdas, A. K. (1977). Piezospectroscopy of the Raman spectrum of  $\alpha$ -quartz. *Physical Review B*, *16*(8), 3815–3826. <https://doi.org/10.1103/PhysRevB.16.3815>
- Busing, W. R., & Levy, H. A. (1967). Angle calculations for 3- and 4-circle X-ray and neutron diffractometers. *Acta Crystallographica*, *22*(4), 457–464. <https://doi.org/10.1107/s0365110x67000970>
- Campomenosi, N., Mazzucchelli, M. L., Mihailova, B. D., Scambelluri, M., Angel, R. J., Nestola, F., et al. (2018). How geometry and anisotropy affect residual strain in host inclusion system: Coupling experimental and numerical approaches. *American Mineralogist*, *103*(12), 2032–2035. <https://doi.org/10.1111/ijlh.1242610.2138/am-2018-6700ccby>
- Campomenosi, N., Rubatto, D., Hermann, J., Mihailova, B., Scambelluri, M., & Alvaro, M. (2020). Establishing a protocol for the selection of zircon inclusions in garnet for Raman thermobarometry. *American Mineralogist*, *105*(7), 992–1001. <https://doi.org/10.2138/am-2020-7246>
- Cesare, B., Parisatto, M., Mancini, L., Peruzzo, L., Franceschi, M., Tacchetto, T., et al. (2021). Mineral inclusions are not immutable: Evidence of post-entrapment thermally-induced shape change of quartz in garnet. *Earth and Planetary Science Letters*, *555*, 116708. <https://doi.org/10.1016/j.epsl.2020.116708>
- Cisneros, M., Ashley, K. T., & Bodnar, R. J. (2020). Evaluation and application of the quartz-inclusions-in-epidote mineral barometer. *American Mineralogist*, *105*(8), 1140–1151. <https://doi.org/10.2138/am-2020-7379>
- Ehlers, A. M., Zaffiro, G., Angel, R. J., Boff-Ballaran, T., Carpenter, M. A., Alvaro, M., & Ross, N. L. (2021). Thermoelastic properties of zircon: Implications for geothermobarometry. *American Mineralogist*. <https://doi.org/10.2138/am-2021-7731>
- Enami, M., Nishiyama, T., & Mouri, T. (2007). Laser Raman microspectrometry of metamorphic quartz: A simple method for comparison of metamorphic pressures. *American Mineralogist*, *92*(8–9), 1303–1315. <https://doi.org/10.2138/am.2007.2438>
- Eshelby, J. D. (1957). The determination of the elastic field of an ellipsoidal inclusion, and related problems. *Proceedings of the Royal Society of London-Series A: Mathematical and Physical Sciences*, *241*(1226), 376–396. <https://doi.org/10.1098/rspa.1957.0133>
- Ferrero, S., & Angel, R. J. (2018). Micropetrology: Are inclusions grains of truth? *Journal of Petrology*, *59*(9), 1671–1700. <https://doi.org/10.1093/ptrology/egy075>
- Gilio, M., Angel, R. J., & Alvaro, M. (2021). Elastic geobarometry: How to work with residual inclusion strains and pressures. *American Mineralogist*. <https://doi.org/10.2138/am-2021-7928>
- Gonzalez, J. P., Baldwin, S. L., Thomas, J. B., Nachlas, W. O., & Fitzgerald, P. G. (2020). Evidence for ultrahigh-pressure metamorphism discovered in the appalachian orogen. *Geology*, *48*(10), 949–951. <https://doi.org/10.1130/G47507.1>
- Gonzalez, J. P., Thomas, J. B., Baldwin, S. L., & Alvaro, M. (2019). Quartz-in-garnet and Ti-in-quartz thermobarometry: Methodology and first application to a quartzofeldspathic gneiss from eastern Papua New Guinea. *Journal of Metamorphic Geology*, *37*, 1193–1208. <https://doi.org/10.1111/jmg.12508>
- Guiraud, M., & Powell, R. (2006). P–V–T relationships and mineral equilibria in inclusions in minerals. *Earth and Planetary Science Letters*, *244*(3–4), 683–694. <https://doi.org/10.1016/j.epsl.2006.02.021>
- Guo, J., Zheng, J., Cawood, P. A., Weinberg, R. F., Ping, X., & Li, Y. (2021). Archean trondhjemitic crust at depth in yangtze craton: Evidence from TTG xenolith in mafic dyke and apatite inclusion pressure in zircon. *Precambrian Research*, *354*, 106055. <https://doi.org/10.1016/j.precamres.2020.106055>
- Korsakov, A. V., Kohn, M. J., & Perraki, M. (2020). Applications of Raman spectroscopy in metamorphic petrology and tectonics. *Elements*, *16*(2), 105–110. <https://doi.org/10.2138/gselements.16.2.105>

- Lakshantov, D. L., Sinogeikin, S. V., & Bass, J. D. (2007). High-temperature phase transitions and elasticity of silica polymorphs. *Physics and Chemistry of Minerals*, 34(1), 11–22. <https://doi.org/10.1007/s00269-006-0113-y>
- Mazzucchelli, M. L., Burnley, P., Angel, R. J., Morganti, S., Domeneghetti, M. C., Nestola, F., & Alvaro, M. (2018). Elastic geothermobarometry: Corrections for the geometry of the host-inclusion system. *Geology*, 46(3), 231–234. <https://doi.org/10.1130/G39807.1>
- Mazzucchelli, M. L., Reali, A., Morganti, S., Angel, R. J., & Alvaro, M. (2019). Elastic geobarometry for anisotropic inclusions in cubic hosts. *Lithos*, 350–351, 105218. <https://doi.org/10.1016/j.lithos.2019.105218>
- Morganti, S., Mazzucchelli, M. L., Alvaro, M., & Reali, A. (2020). A numerical application of the Eshelby theory for geobarometry of non-ideal host-inclusion systems. *Meccanica*, 55(4), 751–764. <https://doi.org/10.1007/s11012-020-01135-z>
- Moulas, E., Kostopoulos, D., Podladchikov, Y., Chatzitheodoridis, E., Schenker, F. L., Zingerman, K. M., et al. (2020). Calculating pressure with elastic geobarometry: A comparison of different elastic solutions with application to a calc-silicate gneiss from the rhodope metamorphic province. *Lithos*, 378–379, 105803. <https://doi.org/10.1016/j.lithos.2020.105803>
- Murri, M., Mazzucchelli, M. L., Campomenosi, N., Korsakov, A. V., Prencipe, M., Mihailova, B. D., et al. (2018). Raman elastic geobarometry for anisotropic mineral inclusions. *American Mineralogist*, 103(11), 1869–1872. <https://doi.org/10.2138/am-2018-662SCCBY>
- Nestola, F. (2020). The role of elastic anisotropy in determining the depth of formation for diamonds and their inclusions. *Rendiconti Lincei*, 31, 285–293. <https://doi.org/10.1007/s12210-020-00897-8>
- Nimis, P., Alvaro, M., Nestola, F., Angel, R. J., Marquardt, K., Rustioni, G., et al. (2016). First evidence of hydrous silicic fluid films around solid inclusions in gem-quality diamonds. *Lithos*, 260, 384–389. <https://doi.org/10.1016/j.lithos.2016.05.019>
- Nye, J. F. (1985). *Physical properties of crystals*. Oxford University Press.
- Özkan, H., Cartz, L., & Jamieson, J. C. (1974). Elastic constants of nonmetamict zirconium silicate. *Journal of Applied Physics*, 45(2), 556–562. <https://doi.org/10.1063/1.1663283>
- Rosenfeld, J. L., & Chase, A. B. (1961). Pressure and temperature of crystallization from elastic effects around solid inclusions in minerals? *American Journal of Science*, 259, 519–541. <https://doi.org/10.2475/ajs.259.7.519>
- Schlenker, J. L., Gibbs, G. V., & Boisen, M. B. (1978). Strain-tensor components expressed in terms of lattice parameters. *Acta Crystallographica Section A*, 34(1), 52–54. <https://doi.org/10.1107/S0567739478000108>
- Schoene, B. (2013). U-Th-Pb geochronology. In *Treatise on geochemistry* (2nd ed., Vol. 4). <https://doi.org/10.1016/B978-0-08-095975-7.00310-7>
- Spear, F. S., Thomas, J. B., & Hallett, B. W. (2014). Overstepping the garnet isograd: A comparison of QuiG barometry and thermodynamic modeling. *Contributions to Mineralogy and Petrology*, 168(3), 1059. <https://doi.org/10.1007/s00410-014-1059-6>
- Spear, F. S., & Wolfe, O. M. (2020). Reevaluation of “equilibrium” P-T paths from zoned garnet in light of quartz inclusion in garnet (QuiG) barometry. *Lithos*, 372–373, 105650. <https://doi.org/10.1016/j.lithos.2020.105650>
- Taguchi, T., Igami, Y., Miyake, A., & Enami, M. (2019). Factors affecting preservation of coesite in ultrahigh-pressure metamorphic rocks: Insights from TEM observations of dislocations within kyanite. *Journal of Metamorphic Geology*, 37(3), 401–414. <https://doi.org/10.1111/jmg.12470>
- Thomas, J. B., & Spear, F. S. (2018). Experimental study of quartz inclusions in garnet at pressures up to 3.0 GPa: Evaluating validity of the quartz-in-garnet inclusion elastic thermobarometer. *Contributions to Mineralogy and Petrology*, 173(5), 42. <https://doi.org/10.1007/s00410-018-1469-y>
- Watson, E. B., & Harrison, T. M. (2005). Zircon thermometer reveals minimum melting conditions on earliest earth. *Science*, 308, 841–844. <https://doi.org/10.1126/science.1110873>
- Wolfe, O. M., & Spear, F. S. (2020). Regional quartz inclusion barometry and comparison with conventional thermobarometry and intersecting isopleths from the connecticut valley trough, vermont and massachusetts, USA. *Journal of Petrology*, 61(8), egaa076. <https://doi.org/10.1093/petrology/egaa076>
- Zhang, Y. (1998). Mechanical and phase equilibria in inclusion—Host systems. *Earth and Planetary Science Letters*, 157, 209–222. [https://doi.org/10.1016/S0012-821X\(98\)00036-3](https://doi.org/10.1016/S0012-821X(98)00036-3)
- Zhong, X., Andersen, N. H., Dabrowski, M., & Jamtviet, B. (2019). Zircon and quartz inclusions in garnet used for complimentary Raman-thermobarometry: Application to the holsnøy eclogite, Bergen Arcs, Western Norway. *Contributions to Mineralogy and Petrology*, 174(6), 50. <https://doi.org/10.1007/s00410-019-1584-4>
- Zhong, X., Dabrowski, M., & Jamtveit, B. (2020a). Analytical solution for residual stress and strain preserved in anisotropic inclusion entrapped in isotropic host. *Solid Earth*, 12, 817–833. <https://doi.org/10.5194/se-2020-180>
- Zhong, X., Moulas, E., & Tajčmanová, L. (2018). Tiny timekeepers witnessing high-rate exhumation processes. *Scientific Reports*, 8(1), 2234. <https://doi.org/10.1038/s41598-018-20291-7>
- Zhong, X., Moulas, E., & Tajčmanová, L. (2020b). Post-entrapment modification of residual inclusion pressure and its implications for Raman elastic thermobarometry. *Solid Earth*, 11, 223–240. <https://doi.org/10.5194/se-11-223-2020>

## References From the Supporting Information

- Angel, R. J., Jackson, J. M., Reichmann, H. J., & Speziale, S. (2009). Elasticity measurements on minerals: A review. *European Journal of Mineralogy*, 21(3), 525–550. <https://doi.org/10.1127/0935-1221/2009/0021-1925>
- ANSI/IEEE. (1987). ANSI/IEEE Std 176-1987 An American National (Vol. 74). Standard IEEE Standard on Piezoelectricity.
- Ranganathan, S. I., & Ostoja-Starzewski, M. (2008). Universal elastic anisotropy index. *Physical Review Letters*, 101(5), 3–6. <https://doi.org/10.1103/PhysRevLett.101.055504>
- Voigt, W. (1910). *Lehrbuch der Kristallphysik*. Kristallographik. Teubner.